Inorganic Chemistry

pubs.acs.org/IC Article

Synthesis, Structure, and Luminescence of Mixed-Ligand Lanthanide Trifluoroacetates

Hashini N. Munasinghe, Regina G. Szlag, Marcos R. Imer, and Federico A. Rabuffetti*



Cite This: Inorg. Chem. 2022, 61, 5588-5594



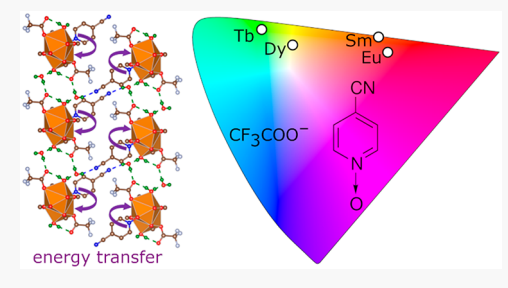
ACCESS I

Metrics & More

Article Recommendations

SI Supporting Information

ABSTRACT: A series of new mixed-ligand lanthanide trifluoroacetates of formula $Ln(4\text{-cpno})(tfa)_3(H_2O)\cdot H_2O$ (Ln = Sm, Eu, Gd, Tb, Dy; 4-cpno = 4-cyanopyridine *N*-oxide; tfa = trifluoroacetate) is reported. Trifluoroacetates were synthesized as chemically pure polycrystalline solids and their crystal structures were probed using single-crystal and powder X-ray diffraction. $Ln(4\text{-cpno})(tfa)_3(H_2O)\cdot H_2O$ solids make up an isostructural series in which LnO_8 polyhedra are bridged by 4-cpno to form edge-sharing dimers. Trifluoroacetato connects these dimers to yield chains whose three-dimensional packing is governed by hydrogen bonds established between 4-cpno, trifluoroacetato, and water. 4-cpno serves as an efficient sensitizer of lanthanide-centered luminescence. UV excitation



of its singlet manifold and subsequent energy transfer to the 4f levels of the lanthanides yield orange (Sm), red (Eu), green (Tb), and yellow (Dy) emissions. Sensitization efficiencies reach 81 and 64% for Eu and Tb hybrids, respectively. Tb(4-cpno)(tfa) $_3$ (H $_2$ O)·H $_2$ O displays a quantum yield of 52%, which coupled to the high absorptivity of 4-cpno, makes it a bright-green emitter under 292 nm excitation. Lanthanide trifluoroacetates may therefore serve as hybrid solid-state light emitters provided that adequate sensitizers are identified.

■ INTRODUCTION

Lanthanide trifluoroacetates of formula Ln(tfa)₃(H₂O)₃ (lanthanide Ln = Y; tfa = trifluoroacetate) are routinely employed in the synthesis of downconverting and upconverting phosphors such as LnF₃ and NaLnF₄.^{1,2} Ln(tfa)₃(H₂O)₃ belongs to the family of mono- and bimetallic trifluoroacetates whose reactivity as fluorinated precursors to single- and mixedmetal fluorides is well-established. 3-10 By contrast, the potential of trifluoroacetates as hybrid organic-inorganic solid-state emitters has been largely overlooked. In the case of Ln(tfa)₃(H₂O)₃, this gap stems from (1) the low absorptivity of 4f-4f transitions, which leads to weak luminescence upon direct excitation of trivalent lanthanides, (2) the very large energy gap between the singlet and triplet states of the trifluoroacetate anion (>13000 cm⁻¹), 11-13 which prevents it from acting as an efficient sensitizer of lanthanide luminescence via intersystem crossing followed by triplet-to-4f energy transfer, and (3) water molecules directly coordinated to the lanthanide ion, which tend to quench luminescence via multiphonon relaxation of the excited 4f levels. With the aim of addressing these issues, auxiliary ligands that sensitize lanthanide emission and displace coordinated water molecules may be incorporated into the crystal structure of lanthanide trifluoroacetates. This strategy is commonly used in the design and synthesis of mono- and polynuclear luminescent lanthanide complexes. 14 Following this approach, mixed-ligand lanthanide trifluoroacetates featuring 2,2'-bipyridine, ¹³,15-17 1,10-phenanthroline, ¹³,15,16 diphenylguanidine, ¹⁶ tris[3-(2'pyridyl)pyrazolyl]borate, 12 triphenylphosphine oxide, 1

hexamethylphosphotriamide¹⁵ have been synthesized. Unfortunately, these studies did not report luminescence quantum yields and sensitization efficiencies. Both metrics are critical to gauge the potential of an auxiliary ligand as a sensitizer and, ultimately, to design bright hybrid emitters.

In this Article, we extend the functionality of lanthanide trifluoroacetates to solid-state light emission. We report the synthesis, structure, and luminescence of a series of new mixed-ligand trifluoroacetates of formula $Ln(4\text{-cpno})(tfa)_3(H_2O)\cdot H_2O$ (Ln = Sm, Eu, Gd, Tb, Dy; 4-cpno = 4-cyanopyridine Noxide). The choice of 4-cpno as a light harvester is based on previous studies of mixed-ligand lanthanide diketonates. ^{18,19} The crystal structures of $Ln(4\text{-cpno})(tfa)_3(H_2O)\cdot H_2O$ hybrids are probed in single-crystal and polycrystalline forms. Their chemical purity is established through Rietveld analysis of powder X-ray diffraction data and thermal analyses. Finally, steady-state and time-resolved spectrofluorometric analyses are carried out to characterize the luminescence response of $Ln(4\text{-cpno})(tfa)_3(H_2O)\cdot H_2O$, including quantum yields and sensitization efficiencies.

Received: January 19, 2022 Published: March 28, 2022





EXPERIMENTAL SECTION

Synthesis. All experiments were carried out under nitrogen atmosphere using standard Schlenk techniques. Sm₂O₃ (99.9%), Eu₂O₃ (99.9%), Gd₂O₃ (99.9%), Tb₂O₃ (99.99%), Dy₂O₃ (99.9%), 4cyanopyridine N-oxide (4-cpno; 96%), and anhydrous CF₃COOH (tfaH; 99%) were purchased from Sigma-Aldrich and used without further purification. Double-distilled water was employed as a cosolvent. Ln(4-cpno)(tfa)3(H2O)·H2O was obtained via solvent evaporation.5 Briefly, Ln₂O₃ (1 mmol), 1.5 mL of tfaH, and 1.5 mL of double-distilled water were added to a 50 mL two-necked roundbottom flask. The resulting suspension was heated at 65 °C for 12 h under air to obtain a colorless, transparent solution. Then, 1 mmol of 4-cpno was added and the mixture was stirred for a few minutes until complete dissolution was achieved. The flask containing the reaction mixture was immersed in a sand bath and solvent evaporation took place at 30 °C for 48 h under a constant flow of dry nitrogen (140 mL min⁻¹). White or off-white polycrystalline solids were thus obtained. Single crystals were recovered from these solids for structure determination. An identical procedure was followed to synthesize Ln(tfa)₃(H₂O)₃, the only difference being that no 4-cpno was added to the reaction mixture. All solids were stored under a static nitrogen atmosphere.

Single-Crystal X-ray Diffraction (SCXRD). SCXRD analysis was carried out using a Bruker X8 Apex diffractometer. A colorless crystal of $Sm(4\text{-cpno})(tfa)_3(H_2O)\cdot H_2O$ (Table 1) with approximate

Table 1. Crystal and Structural Determination Data of Sm(4-cpno)(tfa)₃(H₂O)·H₂O

chemical formula	Sm(4-cpno)(tfa) ₃ (H ₂ O)·H ₂ O
formula weight (g)	645.55
crystal system	triclinic
space group	$P\overline{1}$
a, b, c (Å)	8.1721(4), 10.4996(5), 12.3137(6)
α , β , γ (deg)	92.809(2), 107.637(2), 102.632(2)
volume (ų)	974.95(8)
Z	2
$R[F^2 > 2\sigma(F^2)]$	3.3%
$wR(F^2)$	6.8%
S	1.04

dimensions 0.48 \times 0.32 \times 0.25 mm was selected for structure determination and mounted in Paratone N oil. X-ray intensities were measured at 100 K using Mo K α radiation ($\lambda = 0.71073$ Å). Frames were integrated using Bruker SAINT. Experimental data were corrected for Lorentz, polarization, and absorption effects; for the latter, the multiscan method was employed using Bruker SADABS.²⁰ Structure solution was accomplished using a dual-space approach, as implemented in SHELXT²¹ and difference Fourier (ΔF) maps as embedded in SHELXL-2014/ 7^{22} running under ShelXle.²³ VESTA was used to visualize the resulting crystal structure.²⁴ Hydrogen-atom positions were observed within the first twenty unexplained difference electron density maxima in ΔF maps and refined (i) riding on the parent carbon atoms of 4-cpno, or (ii) with restrained O-H bond distances (0.83(2) Å) and H-O-H angles (1.33(4) Å H···H distance) in the case of water. Isotropic displacement parameters $(U_{\rm iso}^{\rm H})$ of hydrogen atoms in 4-cpno and water were constrained according to $U_{\rm iso}^{\rm H}=1.2\times U_{\rm eq}^{\rm C}$ and $U_{\rm iso}^{\rm H}=1.5\times U_{\rm eq}^{\rm O}$, respectively, where $U_{\rm eq}^{\rm C}$ is the equivalent isotropic displacement parameter of the parent carbon atom and $U_{\rm eq}^{\rm O}$ is the equivalent isotropic displacement parameter of the parent oxygen atom. Table 1 summarizes the crystal data for Sm(4-cpno)(tfa)₃(H₂O)·H₂O. Full details on the data collection and structure refinement are given in the Supporting Information (Tables S1-S5 and Figure S1). Crystal data were deposited in the Cambridge Crystallographic Data Centre with number 2130873.

Powder X-ray Diffraction (PXRD). PXRD patterns of Ln(4-cpno)(tfa)₃(H₂O)·H₂O were collected using a Bruker D2 Phaser

diffractometer operated at 30 kV and 10 mA. Cu $K\alpha$ radiation (λ = 1.5418 Å) was employed. Patterns were collected in the 5–70° 2θ range using a step size of 0.01° and a step time of 1.4 s. **Rietveld Analysis.** Rietveld analyses^{2,5,26} of PXRD patterns were

Rietveld Analysis. Rietveld analyses^{25,26} of PXRD patterns were carried out using the General Structure Analysis System with the graphical user interphase (EXPGUI). The following parameters were refined: (1) scale factor; (2) background, which was modeled using a shifted Chebyschev polynomial function; (3) peak shape, which was modeled using a modified Thompson–Cox–Hasting pseudo-Voight function; (4) lattice constants; (5) atomic coordinates of the lanthanide atom; (6) atomic coordinates of 4-cpno and trifluoroacetato ligands, with each group considered to be a rigid body; (7) an isotropic displacement parameter for the lanthanide atom $(U_{\rm iso}^{\rm Ln})$; (8) an isotropic displacement parameter for all H, C, N, O, and F atoms belonging to 4-cpno, trifluoroacetato, and water $(U_{\rm iso}^{\rm X})$ with the constraint that $U_{\rm iso}^{\rm X}=1.5\times U_{\rm iso}^{\rm Ln}$. Difference curves and $R_{\rm wp}$ residuals were employed to assess the quality of the refined structural models.

Thermal Analyses. Thermogravimetric (TGA) and differential thermal (DTA) analyses were conducted under flowing nitrogen (100 mL min $^{-1}$) using an SDT2960 TGA−DTA analyzer (TA Instruments). ≈5−15 mg of sample were placed in an alumina crucible, held at 35 °C for 30 min, ramped to 600 °C at a rate of 10 °C min $^{-1}$, and kept at that temperature for 30 min.

Spectrofluorometry. Spectrofluorometric analyses were conducted using a Fluorolog 3-222 fluorometer (Horiba Scientific). Room-temperature excitation and emission spectra of Ln(4-cpno)-(tfa)₃(H₂O)·H₂O were collected using a 450 W xenon lamp as the excitation source and a photomultiplier tube R928 as the detector. Slit widths ranged from 1 to 3 nm. Phosphorescence spectra of Gd(4cpno)(tfa)₃(H₂O)·H₂O and Gd(tfa)₃(H₂O)₃ were recorded at 78 K. To this end, powder samples were loaded into a VPF-800 variabletemperature stage (Lake Shore Cryotronics) and degassed at room temperature for 12 h under vacuum (≈80 mTorr). A xenon flashlamp was used as the excitation source. Slit widths were set equal to 1 nm. Luminescence decays were recorded using 290, 370, and 390 nm SpectraLEDs (Horiba Scientific) as excitation sources. Quantum yields were determined using an 80 mm integrating sphere (Horiba Scientific). BaSO₄ (99.9%, Sigma-Aldrich) was used as a blank. Ln(4cpno)(tfa)₃(H₂O)·H₂O samples were diluted in BaSO₄ (≈3 wt %). Fluorescence emission was collected between 400 and 750 nm. Emission spectra were corrected for lamp power fluctuations, detector sensitivity, and integrating sphere response.

UV–Vis Diffuse-Reflectance Spectroscopy. Diffuse-reflectance spectra of $Gd(4\text{-cpno})(tfa)_3(H_2O)\cdot H_2O$ and $Gd(tfa)_3(H_2O)_3$ were collected using a Jasco V-570 UV–vis–NIR spectrophotometer featuring a 60 mm integrating sphere. Spectra were recorded between 200 and 800 nm. $BaSO_4$ (99.9%, Sigma-Aldrich) was a used as a reflectance standard. Reflectance (R) was converted to absorbance using the Kubelka–Munk function F(R) ($F(R) = (1-R)^2/2R$). 30

■ RESULTS AND DISCUSSION

The crystal structure of $Sm(4-cpno)(tfa)_3(H_2O)\cdot H_2O$ is shown in Figure 1. All members of the Ln(4-cpno)-(tfa)₃(H₂O)·H₂O series are isostructural. Sm(4-cpno)- $(tfa)_3(H_2O)\cdot H_2O$ crystallizes in the triclinic $P\overline{1}$ space group. Samarium is eight-coordinated by two oxygen atoms from two 4-cpno ligands, five oxygen atoms belonging to five trifluoroacetato groups, and one oxygen-atom donor from water. The coordination geometry corresponds to a distorted square antiprism. Sm-O bond distances range from 2.34 to 2.49 Å. The building block of the structure consists of dimers of edge-sharing SmO₈ polyhedra. Oxygen atoms belonging to 4-cpno bridge the two samarium atoms, which are ≈4.2 Å apart (Figure 1a). Dimers are connected to each other through the carboxylate group of the trifluoroacetato ligands, thus forming infinite chains that run parallel to the a axis. Samarium atoms belonging to adjacent dimers are \approx 4.4 Å apart.

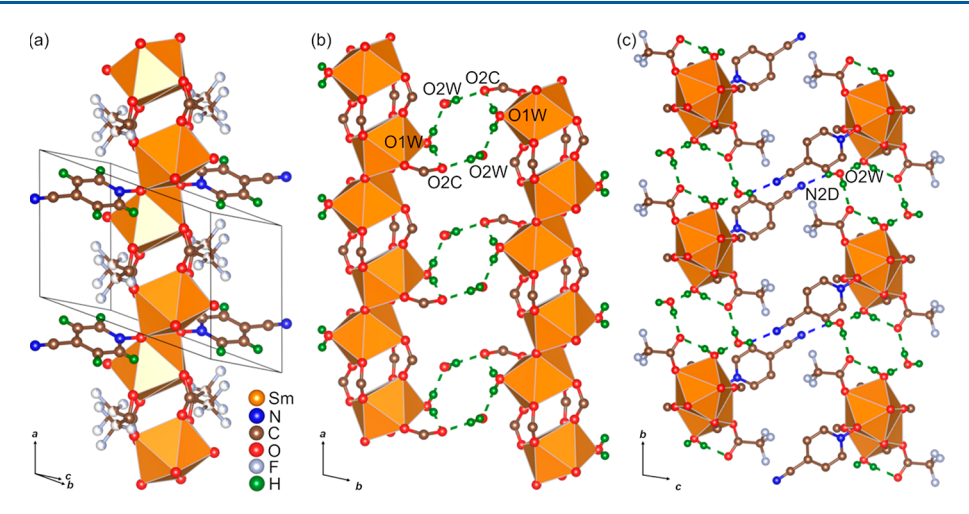


Figure 1. Crystal structure of $Sm(4\text{-cpno})(tfa)_3(H_2O)\cdot H_2O$. (a) Dimers of edge-sharing SmO_8 polyhedra form chains that extend along the a axis. The unit cell of $Sm(4\text{-cpno})(tfa)_3(H_2O)\cdot H_2O$ is shown with solid lines. Splitting of $-CF_3$ groups is omitted for clarity; only major occupancy sites are shown. (b) Hydrogen bonds involving water molecules and trifluoroacetato ligands connect neighboring chains in the ab plane; bonds are depicted with green dashed lines. (c) Three-dimensional connectivity is achieved through hydrogen bonds between crystallization water and 4-cpno; these are depicted with blue dashed lines.

Neighboring chains are held together by a complex network of hydrogen bonds involving water-trifluoroacetato and water-4-cpno interactions. Oxygen atoms O1W (coordinated H₂O), O2W (crystallization H₂O), and O2C (tfa) are involved in these interactions (Figure 1b). Atoms O1W and O2C participate in both intra- and interchain hydrogen bonds. Intrachain bonds are established between O1W (donor) and O2C (acceptor), which are coordinated to the same samarium atom. Interchain bonds involve interactions between O1W (donor) and O2W (acceptor) and between O2W (donor) and O2C (acceptor). The hexagonal ring formed by these hydrogen bonds may be described as R₆(12) using the nomenclature proposed by Etter.³¹ This structural motif leads to the formation of a two-dimensional network of chains extending in the ab plane. Three-dimensional connectivity between chains is provided by hydrogen bonds established between crystallization water (O2W, donor) and 4-cpno (N2D, acceptor; Figure 1c). The above description underscores the key role of crystallization water in determining the packing motif in Sm(4-cpno)(tfa)₃(H₂O)·H₂O because it participates in the two hydrogen-bonding networks that yield the observed three-dimensional crystal structure.

The chemical purity of polycrystalline Ln(4-cpno)-(tfa)₃(H₂O)·H₂O was probed using PXRD and thermal analyses. Results from these studies are summarized in Figure 2 for the case of Sm(4-cpno)(tfa)₃(H₂O)·H₂O. Rietveld refinement of the structure derived from single-crystal analysis provides a good fit to the experimental PXRD pattern (Figure 2a). All diffraction maxima are indexed to Sm(4-cpno)-(tfa)₃(H₂O)·H₂O, demonstrating the phase purity of the polycrystalline solid. This conclusion holds for all other members of the Ln(4-cpno)(tfa)₃(H₂O)·H₂O series (Figure S2). Structural parameters derived from Rietveld analyses are given in Tables S6-S10. Thermal analyses confirm the chemical purity of the samples. Sm(4-cpno)(tfa)₃(H₂O)·H₂O exhibits a total weight loss of ≈68.7 wt % upon heating to 600 °C (Figure 2b). This value is in excellent agreement with the theoretical weight loss expected upon decomposition to SmF₃ (67.8 wt %). Likewise, Eu, Gd, Tb, and Dy compounds exhibit weight losses of \approx 66.6, 64.4, 64.6, and 64.9 wt %, respectively, in good agreement with theoretical values equal to 67.8, 67.2,

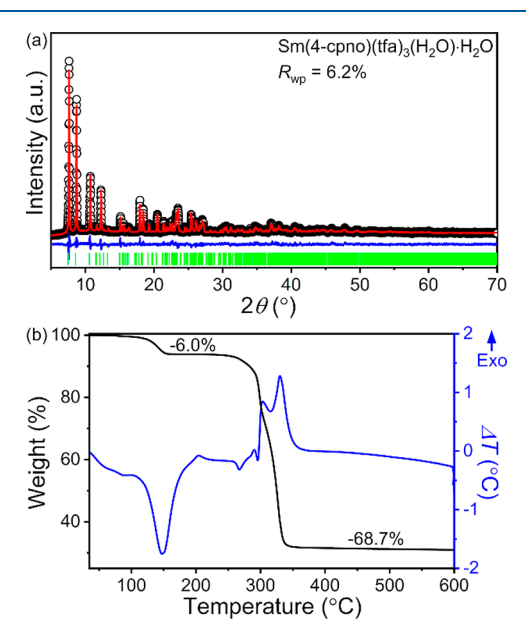


Figure 2. Rietveld (a) and thermal (b) analyses of $Sm(4-cpno)(tfa)_3(H_2O)\cdot H_2O$. Experimental data (O), calculated pattern (red line), difference curve (blue line), and tick marks (green vertical bars) corresponding to the calculated position of the diffraction maxima are shown in (a). Partial and total weight losses are indicated in (b).

67.0, and 66.6 wt % (Figure S3). Thermal decomposition of $Sm(4\text{-cpno})(tfa)_3(H_2O)\cdot H_2O$ entails two major weight losses. The first one occurs around 148 °C and is assigned to the release of water molecules. This assignment is based on (i) the observation of an endothermic peak in the DTA curve and (ii) the agreement between the experimental weight loss and that computed assuming the release of two water molecules (\approx 6.0 vs 5.6 wt %). The second weight loss occurs between \approx 270 and 335 °C. Crystallization of the metal fluoride occurs at \approx 330 °C, as indicated by the exotherm in the DTA curve. Altogether, results from PXRD and TGA/DTA analyses demonstrate that polycrystalline $Ln(4\text{-cpno})(tfa)_3(H_2O)\cdot H_2O$ solids are chemically pure.

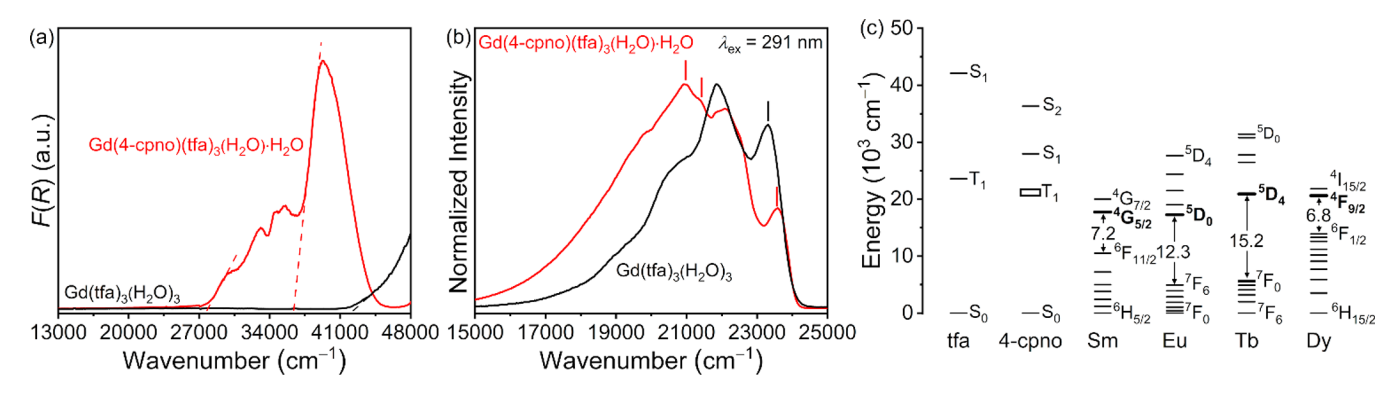


Figure 3. Diffuse-reflectance (a) and phosphorescence emission spectra (b) of $Gd(tfa)_3(H_2O)_3$ and $Gd(4\text{-cpno})(tfa)_3(H_2O) \cdot H_2O$. Dashed lines in (a) indicate absorption edges from which singlet energies are estimated. Tick marks in (b) denote emission peaks used to estimate triplet energies. (c) Energy diagram of selected electronic levels of organic ligands and trivalent lanthanide ions. The main emissive levels of the lanthanide ions are indicated in bold. Energy gaps between these levels and the next lower-lying levels are indicated.

The energies of the lowest-lying singlet and triplet states of the 4-cpno and trifluoroacetate ligands were established prior to investigating the luminescence response of Ln(4-cpno)-(tfa)₃(H₂O)·H₂O. Diffuse-reflectance and phosphorescence spectra of Gd(4-cpno)(tfa)₃(H₂O)·H₂O and Gd(tfa)₃(H₂O)₃ were collected to this end. The energies of singlet states are estimated using the onsets of the absorption edges observed in the reflectance spectra given in Figure 3a. Following this approach, the first excited singlet of tfa may be located at \approx 42100 cm⁻¹ (S₁), in good agreement with previous spectroscopic studies of lanthanide trifluoroacetates. ^{11–13,15,17} In the case of 4-cpno, the first two excited singlets of 4-cpno appear to be located at 27954 cm⁻¹ (S₁, $n \rightarrow \pi^*$) and 36325 cm⁻¹ (S₂, $\pi \to \pi^*$); both values are in excellent agreement with those previously reported for pyridine N-oxide. 32-34 The positions of the lowest-lying triplet states (T1) are estimated using the highest-energy edge of the emission bands observed in the phosphorescence spectra shown in Figure 3b. The spectrum of Gd(tfa)₃(H₂O)₃ exhibits two peaks at 23320 and 21858 cm⁻¹. These are encountered in the spectrum of Gd(4cpno)(tfa)₃(H₂O)·H₂O at 23584 and 22095 cm⁻¹. Additionally, a peak at 20950 cm⁻¹ and a shoulder at 21350 cm⁻¹ are observed in this spectrum. On this basis, the energy of the lowest-lying triplet of tfa in Gd(4-cpno)(tfa)₃(H₂O)·H₂O is estimated to be ≈23320 cm⁻¹, while that of 4-cpno ranges between 20950 and 21350 cm⁻¹. Both values are in good agreement with those reported in the literature. 11,13,18,19 An energy diagram summarizing relevant electronic levels of organic ligands and trivalent lanthanide ions is given in Figure 3c.

The photoluminescence response of polycrystalline Ln(4-cpno)(tfa)₃(H₂O)·H₂O was examined at room temperature. Excitation and emission spectra are shown in Figure 4. Excitation spectra were collected monitoring emissions from Sm, Eu, Tb, and Dy at 597 nm (${}^4G_{5/2} \rightarrow {}^6H_{7/2}$), 612 nm (${}^5D_0 \rightarrow {}^7F_2$), 544 nm (${}^5D_4 \rightarrow {}^7F_5$), and 573 nm (${}^4F_{9/2} \rightarrow {}^6H_{13/2}$), respectively. Both ligand- and metal-centered excitations are observed for all four lanthanides (Figure 4a–d). The broad band extending between 250 and 310 nm is assigned to excitation of the singlet manifold of 4-cpno ($S_0 \rightarrow S_1$, S_2); this band is absent in the excitation spectra of Ln(tfa)₃(H₂O)₃ (Figure S4). f-f excitations, on the other hand, give rise to a series of narrower peaks. The observation of a ligand-centered excitation band while monitoring lanthanide emissions demonstrates sensitization of the latter by 4-cpno. Further,

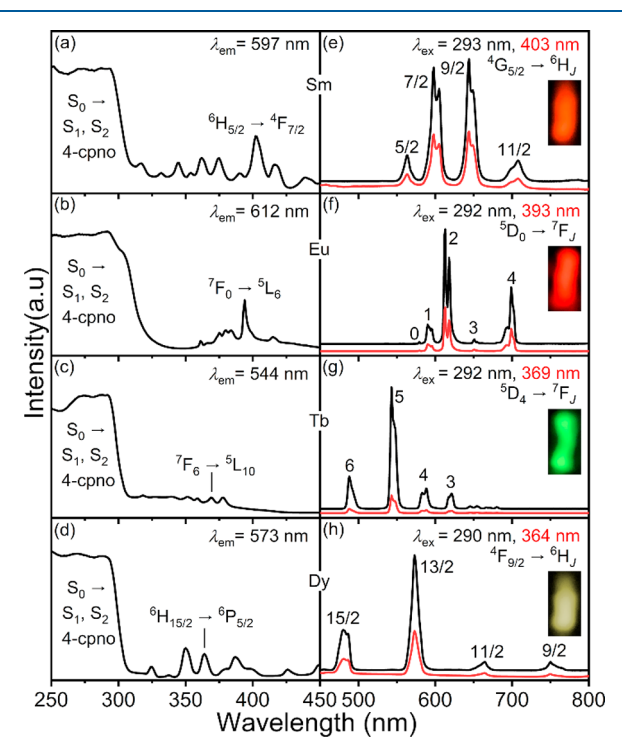


Figure 4. Excitation and emission spectra of $Ln(4\text{-cpno})(tfa)_3(H_2O) \cdot H_2O$. Emission spectra collected under ligand- and lanthanide-centered excitation are shown. Ligand and selected f-f transitions are labeled. Digital pictures of the polycrystalline samples under ligand excitation are given in the insets of panels e-h.

excitation of the 4-cpno ligand results in much higher emission intensities than direct excitation of the lanthanides, indicating good sensitization efficiencies (vide infra). Typically, sensitization of lanthanide ions occurs via energy transfer from the triplet states of the organic ligands to the 4f manifold, ^{18,35-40} although singlets may also be involved. ^{38,41-43} Ligand- and metal-centered excitations of the lanthanide ions result in emissions arising from the ${}^4G_{5/2} \rightarrow {}^6H_J$, ${}^5D_0 \rightarrow {}^7F_J$, ${}^5D_4 \rightarrow {}^7F_J$, and ${}^4F_{9/2} \rightarrow {}^6H_J$ transitions of Sm, Eu, Tb, and Dy, respectively (Figure 4e–h). Ln(4-cpno)(tfa)₃(H₂O)·H₂O solids behave as orange (Sm), red (Eu), green (Tb), and yellow emitters (Dy). The corresponding 1976 CIE chromaticity coordinates are (0.38, 0.54) for Sm, (0.40, 0.51) for Eu, (0.14, 0.56) for Tb, and (0.20, 0.52) for Dy. Details on the calculation of these coordinates and the corresponding colorimetric diagram are

given in the Supporting Information (Figure S5). As expected on the basis of excitation spectra, emissions obtained upon excitation of the 4-cpno ligand are significantly more intense than those obtained via direct excitation, especially in the cases of Eu and Tb compounds. Emission peaks obtained upon direct excitation of Sm and Dy sit on a decreasing background (Figure 4e,h), which we assign to emission from the triplets of the organic ligands. Metal-to-ligand energy transfer therefore occurs in Sm and Dy hybrids but not in their Eu and Tb counterparts, at least not to a noticeable extent. Differences in energy-transfer pathways (and dynamics) between the organic moieties and the 4f manifold of Sm and Dy on the one hand, and Eu and Tb on the other hand, also appear when monitoring the photostability of $Ln(4-cpno)(tfa)_3(H_2O)\cdot H_2O$. Indeed, exposure of Sm and Dy samples to 290 nm excitation for just a few minutes results in an irreversible color change from white to light brown, likely arising from the photodegradation of 4-cpno. 34,44 This color change, which is not observed in Eu and Tb compounds, is accompanied by a noticeable increase in the background signal (Figure S6).

Relevant photophysical parameters of Ln(4-cpno)- $(tfa)_3(H_2O)\cdot H_2O$ are summarized in Table 2. Lifetimes of

Table 2. Photophysical Parameters of Ln(4-cpno)(tfa)₃(H₂O)·H₂O

	$\begin{pmatrix} \lambda_{\mathrm{em}} \\ (\mathrm{nm}) \end{pmatrix}$	$ au_{\mathrm{Ln}}^{\mathrm{L}}~(\mu\mathrm{s}), \ \lambda_{\mathrm{exc}}~(\mathrm{nm})$	$ au_{\mathrm{Ln}}^{\mathrm{Ln}}~(\mu\mathrm{s}),\ \lambda_{\mathrm{exc}}~(\mathrm{nm})$	Q_{Ln}^{L} (%), a,b λ_{exc} (nm)	$Q_{\text{Ln}}^{\text{Ln}}$ (%), a,b λ_{exc} (nm)	$\eta_{ m s} \ (\%)$
Sm	597	1.5, 290	1.9, 390			
Eu	612	643, 290	637, 390	13, 292	16, 393	81
Tb	544	1360, 290	1363, 370	52, 292	81, 369	64
Dy	573	0.85, 290	0.75, 370			

"Measured only for Eu and Tb due to photodegradation of Sm and Dy compounds. b Quantum yields were estimated twice for each sample. Europium trial 1: $Q_{\rm Eu}^{\rm L}=13\%$, $Q_{\rm Eu}^{\rm Eu}=16\%$. Europium trial 2: $Q_{\rm Eu}^{\rm L}=11\%$, $Q_{\rm Tb}^{\rm Eu}=13\%$. Terbium trial 1: $Q_{\rm Tb}^{\rm L}=52\%$ and $Q_{\rm Tb}^{\rm Tb}=81\%$. Terbium trial 2: $Q_{\rm Tb}^{\rm L}=51\%$ and $Q_{\rm Tb}^{\rm Tb}=77\%$. Values from trial 1 were used to compute η_s .

the 597, 612, 544, and 573 nm emissions of Sm, Eu, Tb, and Dy, respectively, were estimated under ligand-centered (τ_{ln}^L) and lanthanide-centered $(au_{ ext{Ln}}^{ ext{Ln}})$ excitation. Likewise, overall (Q_{Ln}^L) and intrinsic (Q_{Ln}^{Ln}) quantum yields were determined. Sensitization efficiencies (η_s) were then computed as the ratio of the overall to intrinsic quantum yields. Luminescence decays are adequately fit using a monoexponential function (Figure S7). In the case of Eu(4-cpno)(tfa)₃(H_2O)· H_2O , however, a slight but noticeable deviation from the monoexponential behavior is observed in the early stages of the decay measured under lanthanide-centered excitation, likely indicating energy transfer between Eu³⁺ ions. Sm and Dy decays are in the (sub)microsecond range, significantly faster than those of Eu and Tb, which occur in the (sub)millisecond range. This difference stems from the much smaller energy gap between the emissive levels of Sm and Dy and the next lower-lying levels of their 4f manifolds (7200 cm⁻¹ for Sm and 6800 cm⁻² for Dy vs 12300 cm⁻¹ for Eu and 15200 cm⁻¹ for Tb; Figure 3c). Smaller energy gaps lead to faster nonradiative relaxation rates due to multiphonon deactivation of the 4f excited levels. In the case of Ln(4-cpno)(tfa)₃(H₂O)·H₂O, the presence of high-energy oscillators such as water molecules coordinated to the lanthanide ions facilitates bridging of this gap. Energy backtransfer to the triplet states of the organic ligands is usually invoked as an additional pathway that decreases the lifetime of

the lanthanide's emissive levels. The rate of back-transfer depends on temperature and on the energy gap between the ligands' triplets and the emissive levels. While this pathway may be operative in $Ln(4-cpno)(tfa)_3(H_2O)\cdot H_2O$, it does not explain the difference observed between the lifetimes of Sm and Dy and those of Eu and Tb because the emissive levels of Sm and Eu are both located $\approx 3500 \text{ cm}^{-1}$ below the triplet state of 4-cpno. A similar argument applies to Tb and Dy because their emissive levels are positioned at nearly the same energy as the triplet of 4-cpno. Regarding overall quantum yields and sensitization efficiencies, values of 13 and 81%, respectively, are obtained for Eu(4-cpno)(tfa)₃(H_2O)· H_2O . In the case of the Tb compound, the overall quantum yield equals 52% and the sensitization efficiency reaches 64%. Similar quantum yield values were reported for dimeric complexes of Eu and Tb featuring hexafluoroacetylacetonate and 4-cpno as ligands (26% for Eu and 49% for Tb). The quantum yield of $Tb(4-cpno)(tfa)_3(H_2O)\cdot H_2O$ under excitation of the 4-cpno ligand is remarkably high considering the presence of two water molecules coordinated to Tb3+. Such a quantum yield and the high extinction coefficient of 4-cpno result in Tb(4cpno)(tfa)₃(H₂O)·H₂O being a bright-green emitter, demonstrating that lanthanide trifluoroacetates may be rendered efficient hybrid solid-state emitters upon introduction of adequate sensitizers.

CONCLUSIONS

A series of new mixed-ligand lanthanide trifluoroacetates of formula $Ln(4-cpno)(tfa)_3(H_2O)\cdot H_2O$ (Ln = Sm, Eu, Gd, Tb, Dy) was synthesized as chemically pure polycrystalline solids. The crystal structure and luminescence response of each member of the series were quantitatively probed. Ln(4cpno)(tfa)₃(H₂O)·H₂O features dimers of edge-sharing lanthanide-oxygen polyhedra. These are bridged by 4-cpno, while trifluoroacetato connects neighboring dimers to yield chains. The three-dimensional packing of these chains is governed by water-trifluoroacetato and water-4-cpno hydrogen bonds. Besides its structural role, 4-cpno acts as an efficient sensitizer of lanthanide-centered luminescence. Orange (Sm), red (Eu), green (Tb), and yellow (Dy) emissions are observed upon UV excitation of the singlet manifold of 4-cpno. Sensitization efficiencies of 81 and 64% are achieved for Eu and Tb hybrids, respectively. Tb(4-cpno)(tfa)₃(H₂O)·H₂O displays an overall quantum yield of 52%, which coupled to the high absorptivity of 4-cpno, leads to bright green emission. Results presented in this Article extend the functionality of lanthanide trifluoroacetates to solid-state light emission. Future work will focus on expanding the library of sensitizer ligands that efficiently transfer energy to lanthanide ions coordinated to trifluoroacetato donors but are not prone to photodegradation.

ASSOCIATED CONTENT

Supporting Information

The Supporting Information is available free of charge at https://pubs.acs.org/doi/10.1021/acs.inorgchem.2c00196.

Crystallographic information of Sm(4-cpno)-(tfa)₃(H₂O)·H₂O, Rietveld and thermal analyses of Ln(4-cpno)(tfa)₃(H₂O)·H₂O, excitation spectra of Ln(tfa)₃(H₂O)₃, calculation of the 1976 CIE chromaticity coordinates and colorimetric diagram, time evolution of Ln(4-cpno)(tfa)₃(H₂O)·H₂O emission under ligand-

centered excitation, and luminescence decays of Ln(4-cpno)(tfa)₃(H₂O)·H₂O (PDF)

Accession Codes

CCDC 2130873 contains the supplementary crystallographic data for this paper. These data can be obtained free of charge via www.ccdc.cam.ac.uk/data_request/cif, or by emailing data_request@ccdc.cam.ac.uk, or by contacting The Cambridge Crystallographic Data Centre, 12 Union Road, Cambridge CB2 1EZ, UK; fax: +44 1223 336033.

AUTHOR INFORMATION

Corresponding Author

Federico A. Rabuffetti — Department of Chemistry, Wayne State University, Detroit, Michigan 48202, United States; orcid.org/0000-0001-8500-3427; Email: far@chem.wayne.edu

Authors

Hashini N. Munasinghe — Department of Chemistry, Wayne State University, Detroit, Michigan 48202, United States Regina G. Szlag — Department of Chemistry, Wayne State University, Detroit, Michigan 48202, United States Marcos R. Imer — Department of Chemistry, Wayne State University, Detroit, Michigan 48202, United States

Complete contact information is available at: https://pubs.acs.org/10.1021/acs.inorgchem.2c00196

Notes

The authors declare no competing financial interest.

ACKNOWLEDGMENTS

The authors acknowledge financial support of the National Science Foundation (Grant DMR-2003118), the Michigan Space Grant Consortium (Grant NNX15AJ20H), and the Department of Chemistry at Wayne State University. They also thank the Lumigen Instrument Center at Wayne State University for use of their single-crystal diffractometer (National Institutes of Health Supplement Grant 3R01EB027103-02S1) and powder diffractometer (National Science Foundation Grant MRI-1427926).

REFERENCES

- (1) Sun, X.; Zhang, Y.-W.; Du, Y.-P.; Yan, Z.-G.; Si, R.; You, L.-P.; Yan, C.-H. From Trifluoroacetate Complex Precursors to Monodisperse Rare-Earth Fluoride and Oxyfluoride Nanocrystals with Diverse Shapes through Controlled Fluorination in Solution Phase. *Chem. Eur. J.* 2007, 13, 2320–2332.
- (2) Mai, H.-X.; Zhang, Y.-W.; Si, R.; Yan, Z.-G.; Sun, L.-d.; You, L.-P.; Yan, C.-H. High-Quality Sodium Rare-Earth Fluoride Nanocrystals: Controlled Synthesis and Optical Properties. *J. Am. Chem. Soc.* **2006**, *128*, 6426–6436.
- (3) Fujihara, S.; Tada, M.; Kimura, T. Controlling Factors for the Conversion of Trifluoroacetate Sols into Thin Metal Fluoride Coatings. J. Sol-Gel Sci. Technol. 2000, 19, 311–314.
- (4) Fujihara, S.; Kadota, Y.; Kimura, T. Role of Organic Additives in the Sol-Gel Synthesis of Porous CaF₂ Anti-Reflective Coatings. *J. Sol-Gel Sci. Technol.* **2002**, *24*, 147–154.
- (5) Dissanayake, K. T.; Mendoza, L. M.; Martin, P. D.; Suescun, L.; Rabuffetti, F. A. Open-Framework Structures of Anhydrous Sr-(CF₃COO)₂ and Ba(CF₃COO)₂. *Inorg. Chem.* **2016**, 55, 170–176.
- (6) Mishra, S.; Daniele, S.; Ledoux, G.; Jeanneau, E.; Joubert, M.-F. Heterometallic Na-Y(Ln) Trifluoroacetate Diglyme Complexes as Novel Single-Source Precursors for Upconverting NaYF₄ Nanocryst-

- als Co-Doped with Yb and Er/Tm Ions. Chem. Commun. 2010, 46, 3756-3758.
- (7) Mishra, S.; Ledoux, G.; Jeanneau, E.; Daniele, S.; Joubert, M.-F. Novel Heterometal-Organic Complexes as First Single Source Precursors for Up-Converting NaY(Ln)F₄ (Ln = Yb, Er, Tm) Nanomaterials. *Dalton Transactions* **2012**, *41*, 1490–1502.
- (8) Dhanapala, B. D.; Munasinghe, H. N.; Suescun, L.; Rabuffetti, F. A. Bimetallic Trifluoroacetates as Single-Source Precursors for Alkali-Manganese Fluoroperovskites. *Inorg. Chem.* **2017**, *56*, 13311–13320.
- (9) Szlag, R. G.; Suescun, L.; Dhanapala, B. D.; Rabuffetti, F. A. Rubidium-Alkaline-Earth Trifluoroacetate Hybrids as Self-Fluorinating Single-Source Precursors to Mixed-Metal Fluorides. *Inorg. Chem.* **2019**, *58*, 3041–3049.
- (10) Munasinghe, H. N.; Suescun, L.; Dhanapala, B. D.; Rabuffetti, F. A. Bimetallic Trifluoroacetates as Precursors to Layered Perovskites A_2MnF_4 (A = K, Rb, and Cs). *Inorg. Chem.* **2020**, *59*, 17268–17275.
- (11) Rastorguev, A. A.; Remova, A. A.; Romanenko, G. V.; Sokolova, N. P.; Belyi, V. I.; Larionov, S. V. Dimeric Structure and Electronic Conformation of Tb(CF₃COO)₃·3H₂O According to Luminescence Data. *Journal of Structural Chemistry* **2001**, *42*, 759–766.
- (12) Mikhalyova, E. A.; Yakovenko, A. V.; Zeller, M.; Gavrilenko, K. S.; Kiskin, M. A.; Smola, S. S.; Dotsenko, V. P.; Eremenko, I. L.; Addison, A. W.; Pavlishchuk, V. V. Crystal Structures and Intense Luminescence of tris(3-(2'-pyridyl)-pyrazolyl)borate Tb³⁺ and Eu³⁺ Complexes with Carboxylate Co-Ligands. *Dalton Transactions* **2017**, *46*, 3457–3469.
- (13) Tsaryuk, V. I.; Vologzhanina, A. V.; Zhuravlev, K. P.; Kudryashova, V. A. Structures and Optical Spectroscopy of Lanthanide Trifluoroacetates Obtained from Hexafluoroacetylacetone. *J. Fluorine Chem.* **2017**, *197*, 87–93.
- (14) Bünzli, J.-C. G. On the Design of Highly Luminescent Lanthanide Complexes. *Coord. Chem. Rev.* **2015**, 293–294, 19–47.
- (15) Kalinovskaya, I. V.; Nikolenko, Y. M.; Karasev, V. E.; Zadorozhnaya, A. N. Fluorescence Properties of Mixed-Ligand Europium Carboxylates. *Russ. J. Inorg. Chem.* **2006**, *51*, 457–461.
- (16) Kalinovskaya, I. V.; Zadorozhnaya, A. N. Gadolinium(III)-Sensitized Fluorescence of Europium in Its Mixed-Metal Compounds with Tifluoroacetate. *J. Mol. Struct.* **2017**, *1134*, 715–721.
- (17) Emelina, T. B.; Kalinovskaya, I. V.; Mirochnik, A. G. Europium(III) Complex with Powerful Antenna Ligands: Interligand Interaction. Spectrochimica Acta Part A: Molecular and Biomolecular Spectroscopy 2019, 207, 222–228.
- (18) Eliseeva, S. V.; Ryazanov, M.; Gumy, F.; Troyanov, S. I.; Lepnev, L. S.; Bünzli, J.-C. G.; Kuzmina, N. P. Dimeric Complexes of Lanthanide(III) Hexafluoroacetylacetonates with 4-Cyanopyridine *N*-Oxide: Synthesis, Crystal Structure, Magnetic and Photoluminescent Properties. *Eur. J. Inorg. Chem.* **2006**, 2006, 4809–4820.
- (19) Eliseeva, S. V.; Kotova, O. V.; Kessler, V. G.; Gumy, F.; Bünzli, J.-C. G.; Kuzmina, N. P. Dimeric Lanthanide Hexafluoroacetylacetonate Adducts with 4-cyanopyridine-N-oxide. *J. Alloys Compd.* **2008**, 451, 414–417.
- (20) Krause, L.; Herbst-Irmer, R.; Sheldrick, G. M.; Stalke, D. Comparison of Silver and Molybdenum Microfocus X-ray Sources for Single-Crystal Structure Determination. *J. Appl. Crystallogr.* **2015**, 48, 3–10
- (21) Sheldrick, G. Crystal Structure Refinement with SHELXL. *Acta Crystallographica Section C* **2015**, 71, 3–8.
- (22) Sheldrick, G. M. SHELXL 2014/7: Program for Crystal Structure Solution; University of Gottingen: Gottingen, Germany, 2014.
- (23) Hubschle, C. B.; Sheldrick, G. M.; Dittrich, B. ShelXle: a Qt Graphical User Interface for SHELXL. *J. Appl. Crystallogr.* **2011**, *44*, 1281–1284.
- (24) Momma, K.; Izumi, F. VESTA 3 for Three-Dimensional Visualization of Crystal, Volumetric and Morphology Data. *J. Appl. Crystallogr.* **2011**, *44*, 1272–1276.
- (25) Rietveld, H. Line Profiles of Neutron Powder-Diffraction Peaks for Structure Refinement. *Acta Crystallogr.* **1967**, 22, 151–152.
- (26) Rietveld, H. A Profile Refinement Method for Nuclear and Magnetic Structures. J. Appl. Crystallogr. 1969, 2, 65–71.

- (27) Larson, A. C.; Von Dreele, R. B. General Structure Analysis System (GSAS); Los Alamos National Laboratory: Los Alamos, NM, 2000.
- (28) Toby, B. EXPGUI, a Graphical User Interface for GSAS. J. Appl. Crystallogr. 2001, 34, 210-213.
- (29) Thompson, P.; Cox, D. E.; Hastings, J. B. Rietveld Refinement of Debye-Scherrer Synchrotron X-ray Data from Al₂O₃. *J. Appl. Crystallogr.* **1987**, *20*, 79–83.
- (30) Kubelka, P.; Munk, F. Ein Beitrag zur Optik der Farbanstriche. Z. Technol. Phys. (Leipzig) 1931, 12, 593-601.
- (31) Etter, M. C. Encoding and Decoding Hydrogen-Bond Patterns of Organic Compounds. *Acc. Chem. Res.* **1990**, 23, 120–126.
- (32) Ito, M.; Hata, N. The Ultra-violet Absorption Spectrum of Pyridine N-oxide. Bull. Chem. Soc. Jpn. 1955, 28, 260–263.
- (33) Ito, M.; Mizushima, W. Analysis of the Near Ultraviolet Absorption Spectrum of Pyridine N-Oxide Vapor. *J. Chem. Phys.* **1956**, 24, 495–500.
- (34) Hata, N.; Tanaka, I. Chemical Processes Subsequent to $n-\pi^*$ and $\pi-\pi^*$ Transitions of Pyridine N-oxide and 2-Picoline N-oxide. *J. Chem. Phys.* **1962**, *36*, 2072–2077.
- (35) Crosby, G. A.; Whan, R. E.; Alire, R. M. Intramolecular Energy Transfer in Rare Earth Chelates. Role of the Triplet State. *J. Chem. Phys.* **1961**, *34*, 743–748.
- (36) Dawson, W. R.; Kropp, J. L.; Windsor, M. W. Internal-Energy-Transfer Efficiencies in Eu³⁺ and Tb³⁺ Chelates Using Excitation to Selected Ion Levels. *J. Chem. Phys.* **1966**, *45*, 2410–2418.
- (37) Latva, M.; Takalo, H.; Mukkala, V.-M.; Matachescu, C.; Rodríguez-Ubis, J. C.; Kankare, J. Correlation Between the Lowest Triplet State Energy Level of the Ligand and Lanthanide(III) Luminescence Quantum Yield. *J. Lumin.* 1997, 75, 149–169.
- (38) Rodríguez-Cortiñas, R.; Avecilla, F.; Platas-Iglesias, C.; Imbert, D.; Bünzli, J.-C. G.; de Blas, A.; Rodríguez-Blas, T. Structural and Photophysical Properties of Heterobimetallic 4f-Zn Iminophenolate Cryptates. *Inorg. Chem.* **2002**, *41*, 5336–5349.
- (39) Yamamoto, M.; Kitagawa, Y.; Nakanishi, T.; Fushimi, K.; Hasegawa, Y. Ligand-Assisted Back Energy Transfer in Luminescent TbIII Complexes for Thermosensing Properties. *Chem. Eur. J.* **2018**, 24, 17719–17726.
- (40) Badiane, A.-M.; Freslon, S.; Daiguebonne, C.; Suffren, Y.; Bernot, K.; Calvez, G.; Costuas, K.; Camara, M.; Guillou, O. Lanthanide-Based Coordination Polymers with a 4,5-Dichlorophthalate Ligand Exhibiting Highly Tunable Luminescence: Toward Luminescent Bar Codes. *Inorg. Chem.* **2018**, *57*, 3399–3410.
- (41) Alaoui, I. M. Nonparticipation of the Ligand's First Triplet State in Intramolecular Energy Transfer in Eu³⁺ and Tb³⁺ Ruhemann's Purple Complexes. *J. Phys. Chem.* **1995**, *99*, 13280–13282.
- (42) Howell, R. C.; Spence, K. V. N.; Kahwa, I. A.; White, A. J. P.; Williams, D. J. The Preparation and Crystal and Molecular Structures of New Luminescent Schiff-Base Complexes Featuring Coupled Lanthanide(III) Cations. *J. Chem. Soc., Dalton Trans.* **1996**, *6*, 961–968.
- (43) Aquino, L. E. d. N.; Barbosa, G. A.; Ramos, J. d. L.; Giese, S. O. K.; Santana, F. S.; Hughes, D. L.; Nunes, G. G.; Fu, L.; Fang, M.; Poneti, G.; Carneiro Neto, A. N.; Moura, R. T.; Ferreira, R. A. S.; Carlos, L. D.; Macedo, A. G.; Soares, J. F. Seven-Coordinate Tb³⁺ Complexes with 90% Quantum Yields: High-Performance Examples of Combined Singlet- and Triplet-to-Tb³⁺ Energy-Transfer Pathways. *Inorg. Chem.* **2021**, *60*, 892–907.
- (44) Bucher, G.; Scaiano, J. C. Laser Flash Photolysis of Pyridine *N*-Oxide: Kinetic Studies of Atomic Oxygen [O(3P)] in Solution. *J. Phys. Chem.* **1994**, *98*, 12471–12473.